Chapter 5

Initial Mn Adsorption and Diffusion Pathways

5.1 Introduction

Spintronics has attracted much attention since it opens the possibility for building up a new class of multi-functional devices. Using the spin of the electron in addition to its charge, creates a remarkable new generation of microelectronic devices. Although this class of material seem very promising, the injection and controlling of spin in semiconductors is still a current topic of research.

Technologically, it would be desirable to grow heterostructures of a transition metal (Mn, Fe, Co, Ni) on the surface of silicon which is the most common semiconductor. This could be done either by depositing a structurally well-defined thin film of a ferromagnetic metal on silicon, or by turning silicon itself into a dilute magnetic semiconductor by adsorption of magnetic metal atoms on the Si. Due to the strong interaction between transition metals and Si surfaces, formation of the intermetallic silicide compounds is energetically preferred on a Si substrate. However, Fe, Co, and Ni silicide films are weakly magnetic or non-magnetic and therefore unsuitable for spintronic devices [85]. On the other hand, Mn displays a considerable magnetic moment in some of its phases. Moreover, both the Mn γ phase and the Mn-silicide compounds have good lattice match to the Si-substrate (see Tab. IV in Chap. 3). Thus, we expect the growth of such films to produce suitable interfaces for spin injection in semiconductors. In analogy to Mn:Ge [123] the possibility to grow strongly doped Mn:Si, which could be ferromagnetic, has been explored theoretically [124, 125]. Recently, it has been shown experimentally that a ferromagnetic phase with a Curie temperature above room temperature can be formed by Mn ion implantation into Si at 0.8% and 0.5% Mn atom concentrations [126, 127].

Another interesting possibility is the growth of heterostructures of Si with Heusler alloy films, e.g., Co_2MnSi or Co_2MnGe. Theses materials that are not only ferromagnetic at room temperature, but also display a high spin polarization of carriers at the Fermi level. Both these properties make this type of materials promising for efficient spin injection of the majority-spin carriers through the heterojunction.

While transition-metal silicide deposition has been studied intensively, only a few experimental studies of Mn-silicide films on Si have been performed. Both metallic MnSi and semiconducting $MnSi_{1.7}$ have been grown [128] on Si(001). Recently experiments also demonstrated the growth of two types of three-dimensional nanostructures on Si(001), which were attributed to MnSi and Mn_5Si_3 nano-crystallites [16]. On the theoretical side, studies of Mn diffusion on Si(001) have not appeared until very recently [124, 125]. However, there are a number of reports, both experimental and theoretical, for other metal atoms on Si(001) [129–131]. In all these cases, dimerization of the adatoms as well as formation of islands and clusters have been observed.

For all these approaches, it is crucial to better understand and control the adsorption, diffusion and nucleation of Mn on the silicon surface. Furthermore in order to identify the elementary growth processes which determine the junction quality, it is essential to have detailed information about the potential energy surface and the possible diffusion paths of Mn on Si.

The current chapter is organized as follows: First the behavior of single Mn adatoms on Si(001), atomic structure, stability, magnetic properties and diffusion pathways will be investigated. Subsequently, the initial growth process of Mn on Si(001) for coverages up to 1 monolayer (ML) will be studied.

5.2 Computational Details

The Si surfaces are modeled using a slab geometry consisting of eight or ten layers of Si atoms for Si(001) and ten or twelve layers for Si(111). Mn adatoms are always placed on both sides of the slab to preserve the inversion symmetry with respect to the middle of the slab. The θ=1 monolayer (ML) coverage of Mn is defined in such a way that it corresponds to a space-filling arrangement of two Mn adatoms per (1×1) unit cell of the Si surface. For Mn coverages $\leq 1/2$ ML on Si(001), the calculations were performed in a $p(2 \times 2)$ unit cell using a surface reconstruction with alternating buckled Si dimers. For Si(111) we performed calculations in a hexagonal (1×1) unit cell containing 1 Mn, which corresponds to a coverage of 0.5 ML. In the case of Si(001), the periodic supercell contains a total of 32 Si atoms in a

eight-layer-slab of Si, plus 1/8 or 1/4 ML of Mn, which corresponds to one or two Mn adsorbed on either side of the supercell. The successive slabs are separated by a vacuum space of 16.4 Å . The Brillouin zone sampling is done by a set of 8 k-points in the irreducible part of the Brillouin zone, derived from a $4\times4\times1$ k-point mesh. In all calculations, the muffin-tin sphere radius is chosen to be 1.11 Å for both Mn and Si. The cut-off energy for the plane-wave expansion in the interstitial region, E_{cut}^{wf}, is 13.8 Ry. The numerical accuracy of the present calculations has been checked by using a higher cut-off energy, *e.g.*, 21.8 Ry, indicating a maximum uncertainty of about 0.1 eV per (1×1) cell for formation energies but negligible change of the relative stability (relative energy difference). All Mn and Si atoms except for the two central-layer Si atoms, were relaxed until the calculated atomic force for each of them is smaller than 0.03 eV / Å.

5.3 Stable and Non-Stable Adatom Positions on The Si(001) Surface

In the following section, the adsorption energy of the single atom adsorption on the Si(001) surface will be reported. The effect of the position of the Mn impurity on the magnetic and electronic properties will be studied as well.

The reported dimer bond lengths is 2.38 Å and the angle of the buckled dimer is around 18.2°. Adsorption of a single Mn atom on this surface leads to the formation of a strong covalent bond, due to the overlap of the two surface states of the dangling bonds with the Mn-d orbitals. This turns the semiconductor behavior of the band structure of the bare surface into a metallic band structure. According to our earlier calculations for bulk Si and Mn-monosilicide, the nearest neighbors interatomic distances are 2.37 Å for Si-Si and 2.38-2.4 Å for Si-Mn. The energy gain to form a Si-Si or a Mn-Si bond are 2.7 eV and 1.3 eV, respectively.

In order to find the binding sites of the Mn atom on the Si(001) surface, the adsorption energy of an adatom is defined as the difference between total energy of the adsorbate and substrate system, E^{tot}, the bare Si(001) surface, $E^{\mathrm{clean}}_{\mathrm{surface}}$ and the free Mn atom, $E^{\mathrm{free}}_{\mathrm{Mn}}$, i.e.

$$E^{\mathrm{ad}} = \frac{1}{2}(E^{\mathrm{tot}} - E^{\mathrm{clean}}_{\mathrm{surface}} - 2E^{\mathrm{free}}_{\mathrm{Mn}}) \tag{5.1}$$

The fraction $\frac{1}{2}$ is considered to count two surfaces in the top and bottom of the slab model.

In Fig 5.1 the most stable adsorption sites on the Si(001) 2×2 reconstructed surface

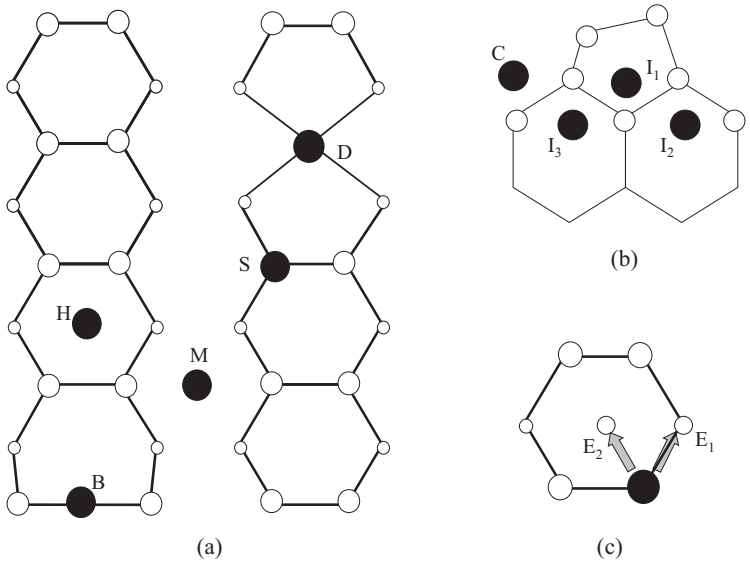

Fig. 5.1: Schematic top view of the Si(001) surface, with various binding sites for a Mn adatom indicated (a). Side view, with sub-surface binding sites of Mn indicated (b). Top view illustrating substitutional adsorption of Mn, the arrows indicating various alternative positions for the expelled Si atom (c). Filled circles indicate possible binding sites for Mn, white circles Si atoms.

are shown. In order to compare the present results to those reported in the literature, the adsorption energies, bonds length and magnetic moments for adatom at some high-symmetry sites of the PES, as well as for some other adsorption geometries are collected in Tab. 5.1. The sites are known as the interstitial (I_1), the third-layer sub-surface (I_2,I_3), the dimer vacancy (D), the cave site (C), the hollow site (H), the substitutional (S), the exchange (E_2,E_3) and the dimer short bridge site (B). The dimer vacancy, 3rd layer sub-surface and interstitial site are stable sites for Co, Ni and Ti adsorption on this surface, respectively [132–134] which induced the idea to include them in the present study[1]. The first three sites are capped by a Si layer. All these geometries which result from an exothermic process are found by fully relaxing the system. The energy of substitutional adsorption of Mn was calculated under the assumption that the replaced Si atom moves to the Si bulk.

The most stable site for Mn is the 2nd-layer tetrahedral interstitial site, I_1. The Mn is located 2 Å below the Si-dimer while it elongates the dimer and moves it up by 1 Å from the surface. This configuration is mentioned also as the lowest energy position in the work of Dalpian, da Silva and Fazzio [124]. In this position, the Mn bonds are completely saturated without disrupting the substrate bonds and the magnetic moment of Mn reduces to $2\,\mu_B$. This is due to strong covalent bonds between

[1]In section 5.4 , the dimer vacancy will be discused in details.

Table 5.1: Bond length of Mn and Si, absolute adsorption energy (eV) and magnetic moment for different adsorption sites for low coverage, $\theta_{\mathrm{Mn}} = 1/8$. Note that the Mn-Si distances are in the range of bond distances known from Mn-monosilicide.

site	Si-Mn Bond Å	E_{ad} eV / atom	Magnetic Moment μ_B
I_1	2.3-2.6	3.80	2.4
D	2.5	4.29	2.9
I_3	2.4-2.5	3.01	2.9
H	2.4	2.91	3.2
S	2.4-2.4	2.86	3.6
B	2.5-2.7	2.72	3.9
E_1	2.3-2.4	2.69	3.0
M	2.4	2.63	4.1
E_2	2.3-2.4	2.36	2.9
C	2.4	2.49	3.3

the adsorbate and substrate atoms. The presence of a Mn atom beneath the dimer, changes the buckled dimer surface into non-buckled and almost symmetric dimer surface. The charge density distribution of this Si-dimer is reduced significantly and is localized around the Mn atom. The dimer bond above Mn is stretched by approximately 16%, whereas the other Si-dimers shrink by about 4% in comparing to the usual Si dimer bond length in bare Si(001) surface. In this optimized atomic configuration, Mn forms 9 bonds with neighboring Si atoms with bond lengths in the range of 2.3 – 2.6 Å.

As seen from the table, the adsorption energy for Mn in the 3rd-layer is less favorable than in the second layer interstitial site. There are two different adsorption sites, I_2 and I_3, in the third layer. Since the dimers are buckled, these two site are not equivalent, i.e. they have different surrounding. The I_2 side is not a real adsorption site since there is no barrier from 3rd layer sub surface I_2 to 2nd layer interstitial, I_1. In this site Mn breaks the Si-dimer's back bonds and diffuses easily to the most stable site, the second layer tetrahedral interstitial site. Mn in the position below the lower Si atom of the dimer, I_3 , has an adsorption energy, E^{ad}, of 3.01 eV. Therefore, the third layer is a thermodynamically unstable place for Mn. From interatomic distances one can conclude that the adsorption in the third layer sites enhances the angle of dimers.

Another metastable adsorption site on the surface is the *pedestal* or *hollowsite* where the Mn is situated between Si-dimers in the same row (in the center of hexagon formed by the surface atoms). Adsorption of Mn on the surface reduces buckling of the dimer, therefore the surface has less distortion. In this metastable

binding site, the Mn atom is in four fold coordination with nearly equally short bonds ($\sim$ 2.4 Å) with Si in the top most layer. The Si-dimers on the substrate still remain intact. The energy gain due to adsorption at this point is about 0.89 eV less compared to the adsorption in the interstitial site I_1.

In the context of epitaxial growth of Mn-doped Si, incorporation of Mn at substitutional positions at the surface is particularly important. This process is likely to trigger silicide formation. On the other hand, it has been long known that the substitutional Mn impurity in Si act as an acceptor [135] with a large local magnetic moment. Hence one could speculate that Si can be turned into a dilute magnetic semiconductor. In the substitutional site, Mn incorporation with a high concentration could be achieved. Therefore, the feasibility of Mn replacing the lower Si atom of the Si surface dimer should be studied. With taking the chemical potential of bulk Si as an energy reference, the substitutional impurity is energetically less favorable than the impurity in the sub-surface interstitial site by 0.93 eV.

In an attempt to calculate the energy barrier for a surface exchange process of Mn and Si, we have calculated several geometries where Mn occupies the Si site, while the replaced Si atom sits at different neighboring positions. Specifically, we investigate the possibilities that the exchanged Si atom could move to an asymmetric position between two Si dimers (marked as E_1 in Fig. 5.1), or to the center of the surface Si-hexagon, the hollow site (marked as E_2 in Fig. 5.1). The adsorption energies for these two possibilities are 0.22 eV and 0.55 eV lower than for a Mn atom in the hollow site. Since the energies of these intermediate configurations can be considered as a lower bound for the energy barrier of substitution, it is concluded that a Mn impurity in the hollow site needs to overcome a barrier of at least 0.22 eV to create a substitutional Mn site at the surface.

However, once a Mn atom has reached the stable interstitial site I_1, the activation energy for creating a substitutional Mn is increased by 0.89 eV. The barrier for reaching the interstitial site from the hollow site is 0.3 eV (see section 5.5.2). Hence we conclude that substitutional and interstitial adsorption of Mn are competing processes.

The Mn impurity at the dimer short bridge site, (B), has the same (x,y) coordinates as the tetrahedral interstitial site, but is located above the Si-dimer. This position is unstable because the Si-Si dimer is broken and the Mn bonds is not saturated. This will cause to diffused Mn to the (H) without any barrier. The impurity in this site is less stable than the I_1 site by 1.07 eV.

The cave site, C, where the Mn atom is located in the trench between two dimer rows, has an adsorption energy of 2.69 eV which is less than for the hollow site impurity by 0.8 eV. In Mn / GaAs(001), where the cave site is a local minimum.

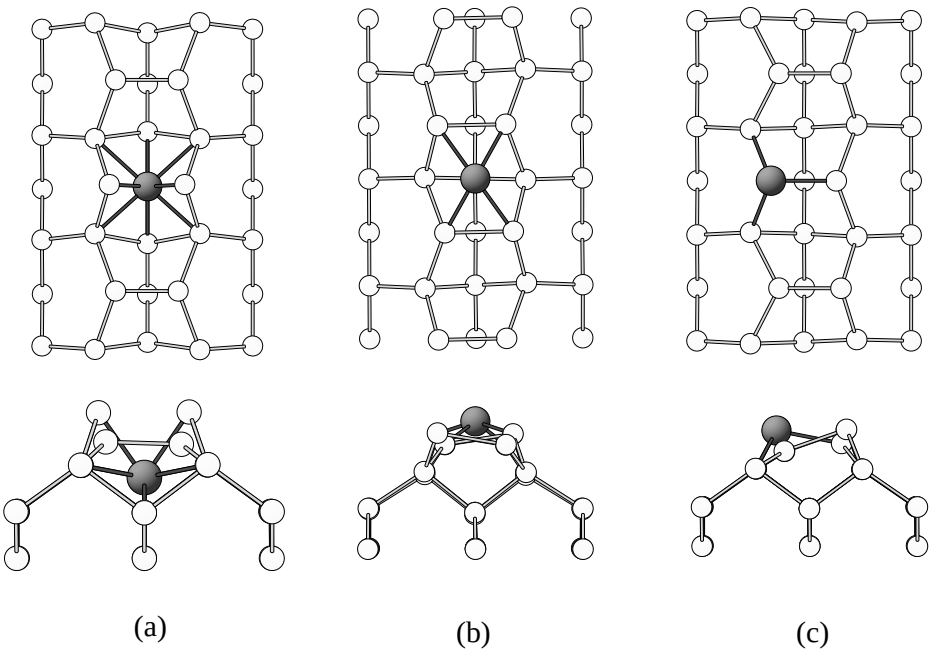

Fig. 5.2: Top view (upper panel) and side view (lower panel) of adsorption of Mn impurity at tetrahedral interstitial site (a), hollow site (b) and substitutional site (c).

In summary we conclude that, due to the strong Mn-Si covalent bonding, incorporation and penetration of a single Mn into silicon sub-surface site is energytically more favorable than adsorption on the surface.

We note that Dalpian *et al.* [124] have performed a similar study, using ultrasoft pseudopotentials and a (4×4) unit cell to describe the surface. In their results, the magnetic moments obtained in the pseudopotential calculations [125] are in fair agreement with ours, except for the second layer interstitial site, where the pseudopotential calculation yields a considerably smaller magnetic moment (0.92 μ_{B}) than our all-electron calculations (2.4 μ_{B}). While the reason of the discrepancy is yet unclear, we note that the magnitude of the magnetic moment may depend sensitively on core polarization effects.

Comparing to recent calculations by Zhu *et al.* for Mn / Ge(001), [123] we conclude that Mn shows very similar behavior on Ge(001) and on Si(001). For Mn on Ge(001), the interstitial sites in deeper layers, as well as the surface substitutional site, are also found to be less stable than the second layer interstitial site, in agreement with the behavior that we find for Mn / Si(001). In similar work by Dalpian *et al.*, the same results were found. In contrast, in Ge the substitutional impurity can diffuse easily to the interstitial impurity [123, 136, 137].

Similarly, calculations for Mn / GaAs(001) have identified the interstitial site below

an As surface dimer to be the most stable site for Mn on GaAs(001). [138]

It is also interesting to compare our results with results for adsorption of other transition metals on Si(001). In a STM study of Cu deposition on Si(001), the Cu atoms form a dimer on top of the Si dimer rows and perpendicular to the Si dimer direction. The adatom dimerization, undimerizes the Si substrate [129]. In a study of the initial process of Ni adsorption, Ni can diffuse rapidly into Si and penetrate to the third sub -surface site [139]. A theoretical study of adsorption of Co on Si(001) predicts that the most stable site for Co is the dimer vacancy which is formed by removing the dimer above cobalt in the site below dimer [132]. For single atom adsorption of Ti, the interstitial site is the most stable site. The adatom adsorbs on a Si-dimer row, dives into the near-surface interstitial site, and the surface Si atoms adjacent to the Ti adatom are ejected on to the terrace [53].

In order to better understand the behavior of Mn in substitutional, tetrahedral interstitial site and hexagonal interstitial site (hollow site), the band structure, DOS and charge density of aforementioned structures will be discused in details.

- **Electronic structures :** For the discussion of the electronic and magnetic properties, it is helpful to look at the band structure of a Mn-impurity at the hollow site, tetrahedral interstitial site and substitutional site, Fig. 5.3. The band structures are plotted in the directions parallel ($\Gamma \rightarrow X$) and perpendicular ($\Gamma \rightarrow Y$) to the surface-dimer. The upper (lower) panel in the Fig. 5.3 are the band structures for the majority (minority) spin channel.

As expected, the magnetic phases are energetically more favorable than the paramagnetic phase. Since the exchange splitting (energy difference between spin up and down state) has a significant effect on the d orbitals, the band structure for spin up and down channels are plotted near the Fermi level where the bands have mainly d character. With comparing the DOS of both spin channels we see, the Si sp orbitals contribute to the bonding state far from the Fermi level and their splitting due to the exchange field is almost negligible.

According to the band structure of the hollow site impurity, both spin channels have semiconductor behavior with a band gap of about 0.42 (0.33) eV for spin up (down) channel (cf. Fig. 5.3-a and d). In contrast, in the substitutional and interstitial site band structures, due to the surface state, the band crosses the Fermi level and is in the shoulder of the peaks. Their band structures have metallic character with spinpolarization of 7% and 51% at the Fermi level for the substitutional and the interstitial impurity, respectively.

Mn in the center of the surface hexagon, hollow site, saturates all surface dangling

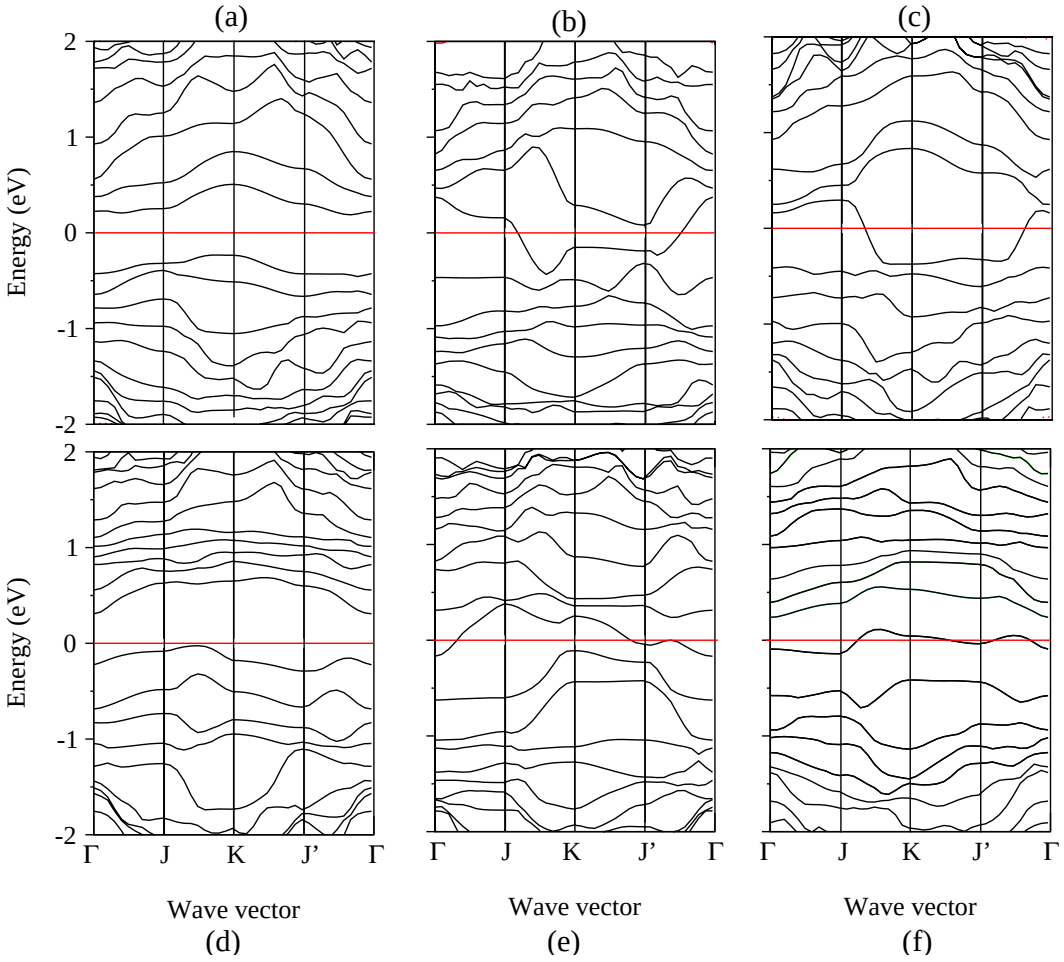

Fig. 5.3: Band structure of up-spin channel (a, b, c) and spin down channel (d, e, f) of a Mn impurity at the hollow, interstitial and substitutional site, respectively.

bounds and opens a gap. While in the interstitial and substitutional structures, the surface bands appear in the band gap where one of them is partially occupied. This band which has relatively large dispersion is responsible for the loss of the band gap.

Since coordination of Mn on the surface is lower than in the bulk, the magnetic moment in the surface becomes higher than bulk Mn. Whenever the exchange splitting is more than the crystal field splitting (energy difference between sub-level of atomic orbital, i.e. d_{e_g} and $d_{t_{2g}}$), therefore a high spin state is observed in the top-most layer, which is in agreement with published calculations [124, 125].

The magnetic moments of Mn in the pedestal and in the substitutional topmost layer are 3.2 and 3.6 μ_{B}, respectively, but for the sub-surface this diminishes to 2.4 μ_{B}. The reduction of the magnetic moment from topmost layer to 2nd layer

is due to the strong overlap between sp-hybridized orbitals of the topmost Si layer and the Mn d-orbitals in the interstitial site which reduces the exchange splitting and hence the magnetic moment. Moreover, due to the different structural environments of Mn atoms at different adsorbtion sites, the population of filled state of d-orbital down-spin channel below the Fermi level in interstitial site is 20% more than hollow and substitutional sites. This induces an increase of the exchange splitting and the magnetic moment in the substitutional (hollow) site in comparison to the interstitial site.

Furthermore, an estimate of the exchange splitting, Δ_x, and the crystal field splitting, $\Delta_{e_g-t_{2g}}$, just for the e_g state at the Γ point in the case of the hollow, substitutional and interstitial site leads to a value of $\Delta_{e_g-t_{2g}} = 0.2, 0.2, 0.1$ eV and $\Delta_x = 3.95, 4.05, 3.25$ eV, respectively.

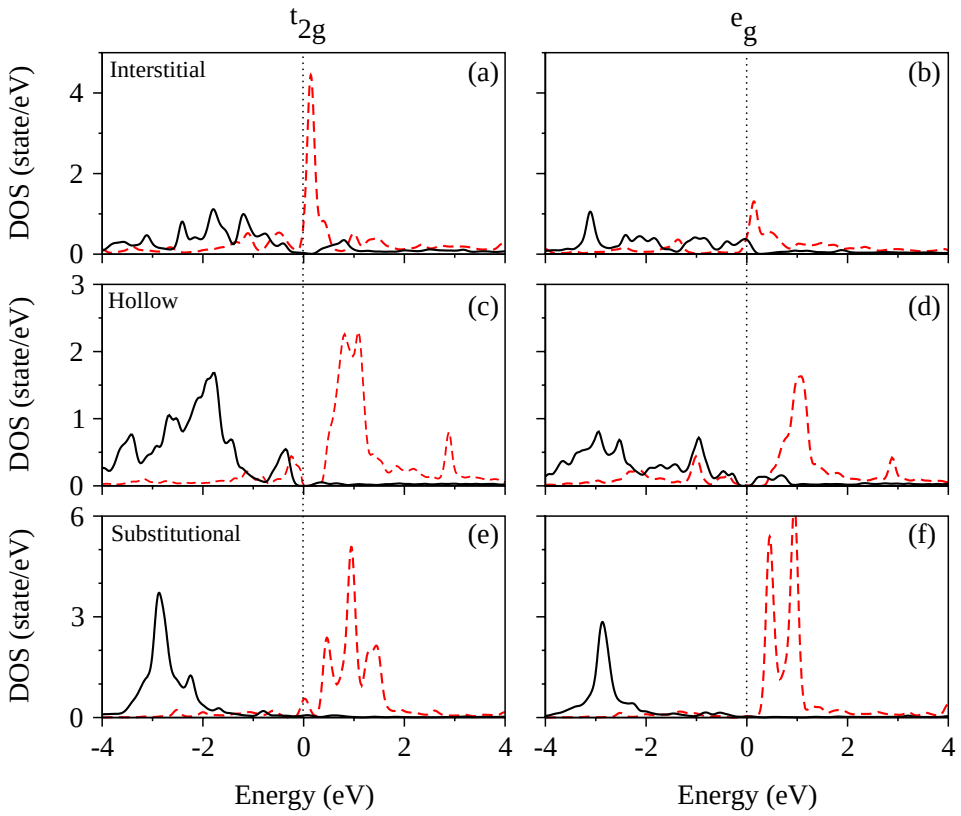

Fig. 5.4: DOS of the $t_{2g} = d_{z^2} + d_{xz} + d_{yz}$ and $e_g = d_{x^2-y^2} + d_{xy}$ sub-levels of partial d-orbitals of a Mn impurity at the tetrahedral interstitial site (a,b), hollow site (c, d) and substitutional site (e, f). Black solid lines are for the majority spin channel and red dashed lines belong to the minority spin channel. The energy zero refers to the Fermi level.

Further insights about magnetic properties can be gained from comparison of the DOS plot for the sub-level of the d-orbitals of Mn at different impurity sites, Fig. 5.4.

Due to the crystal field, the d-orbitals of a Mn atom which is five-fold degenerate splits into a two-fold in-plane d_{e_g}, and three-fold out-of-plane $d_{t_{2g}}$ orbitals. These two levels will be split by an exchange interaction into $d_{x^2-y^2}, d_{xy}$ in-plane and d_{x^2}, d_{xz}, d_{yz} out-of-plane components. The metallic character of the substitutional impurity is mainly due to the out-of-plane $d_{t_{2g}}$ orbitals (specifically d_{xz} and d_{yz} sub-levels), while in the interstitial site both the in-plane d_{e_g} orbitals ($d_{x^2-y^2}$, d_{xy}) and out-of-plane $d_{t_{2g}}$ orbitals (d_{yz} sub-level) are responsible for the metallic behavior.

Since the effect of Mn is evident only starting at about -4 eV below the Fermi level, The comparison of the DOS plots is discussed only in the most affected component at the valence region, near to the Fermi level.

In the interstitial impurity, the well-localized peak for the spin down channel is centered at 0.15 eV and has $d_{t_{2g}}$ character. Whereas in the majority spin channel, the delocalized peaks spread in an energy range from around -4 eV to the Fermi level and correspond to both $d_{t_{2g}}$ and d_{e_g} orbitals.

In contrast, in the majority spin channel of the substitutional site, there is a sharp localized peak centered at 2.85 eV which belongs to $d_{t_{2g}}$ and d_{e_g} sub-levels. The main peaks for minority spin channel are around 1 eV and correspond to both $d_{t_{2g}}$ and d_{e_g} sub-levels.

The band structure for this structure still has metallic behavior which is due to the surface dangling bonds of the second dimer. However, a small gap ($\sim$0.4 eV) appears in the majority spin channel of the DOS of the Mn atom on top of the surface in hollow site. It has 100% spin polarization at the Fermi level.

- **Charge density contour plots :** Comparison of the contour plots of the charge densities for Mn at substitutional, hollow and interstitial sites are the subject of the following part. In Fig. 5.4. , plots (a), (b) and (c) show the contour plot of the charge density in a plane perpendicular to the surface and containing the Mn impurity, and plots (d) and (e) are plotted in a plane parallel to the surface. The white big and small circles are the place of Mn and Si atoms, respectively.

In Mn / Si(001) system, the tilt of the dimers is reduced when the Mn is adsorbed on the surface, especially in the interstitial site. The presence of Mn reduces charge distribution in 2nd, 3rd and fourth layers as well as topmost layer and removes part of the charge from the back bonds. The charge density is mostly confined to the Mn-Si bonds and concentrated around Mn atoms.

In the interstitial and hollow sites, there is still charge density distribution at the place of the upper Si atom which belongs to the dangling bonds.

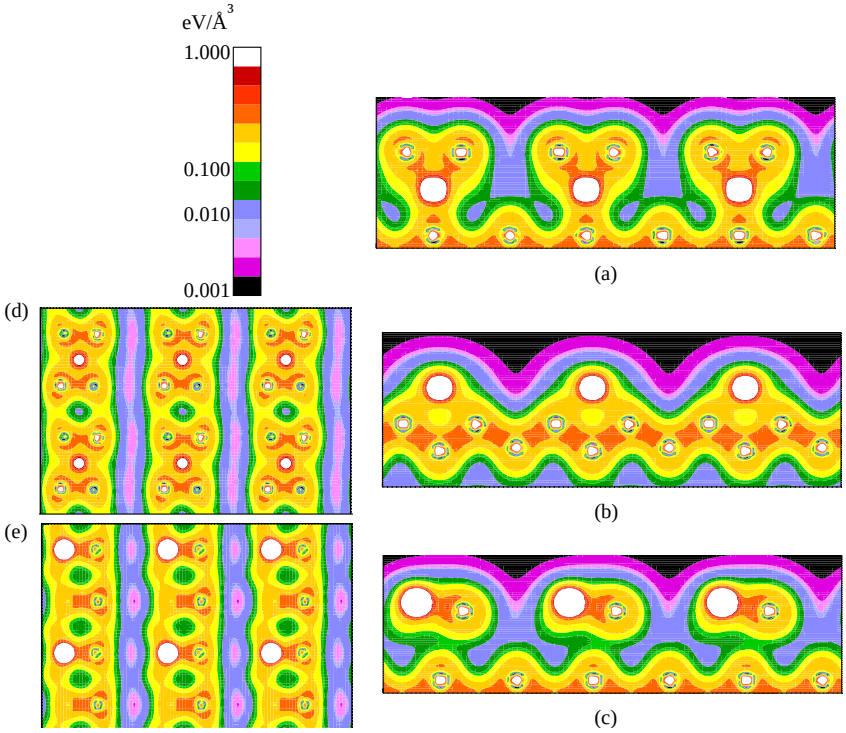

Fig. 5.5: Electron density in the (100) plane containing the adatom for single Mn atom adsorption on substitutional site (a), hollow site (b) and interstitial site (c). The electronic density for the (001) plane (at a certain z above surface) for hollow site (d) and interstitial site (e). The bigger (smaller) white circles in every figure are the places of Mn (Si) atoms.

In the case of Mn adsorption on the substitutional site, the charge density contour plots are similar to those for the bare surface. The itinerant charge is distributed between Mn and the nearest Si and vanishes in the dangling bonds while in the other Si-dimer the dangling bonds are still occupied.

- **STM images :** In order to study the differences between various single Mn atom adsorption sites, the STM for adsorption of $\frac{1}{8}$ ML of Mn at hollow, interstitial in p(2×2) as well as c(4×2)and substitutional site on Si(001) are simulated.

In Fig. 5.6 the simulated STM images for a Mn impurity at the substitutional site(a), the hollow site (b), the tetrahedral interstitial site in a (2×2) cell (c), the tetrahedral interstitial site in a c(4×2) cell (d) and an experimental image (e) [2] are shown.

Besides the decrease of the dimer angle, which can also be seen in charge density contour plots, vanishing of the dangling bonds causes that the bean-like shape of dimers which are observed in the clean Si(001) surface are no longer visible (see Fig.4.10 Chap.4). In all simulated images, the occupied states have a maximum

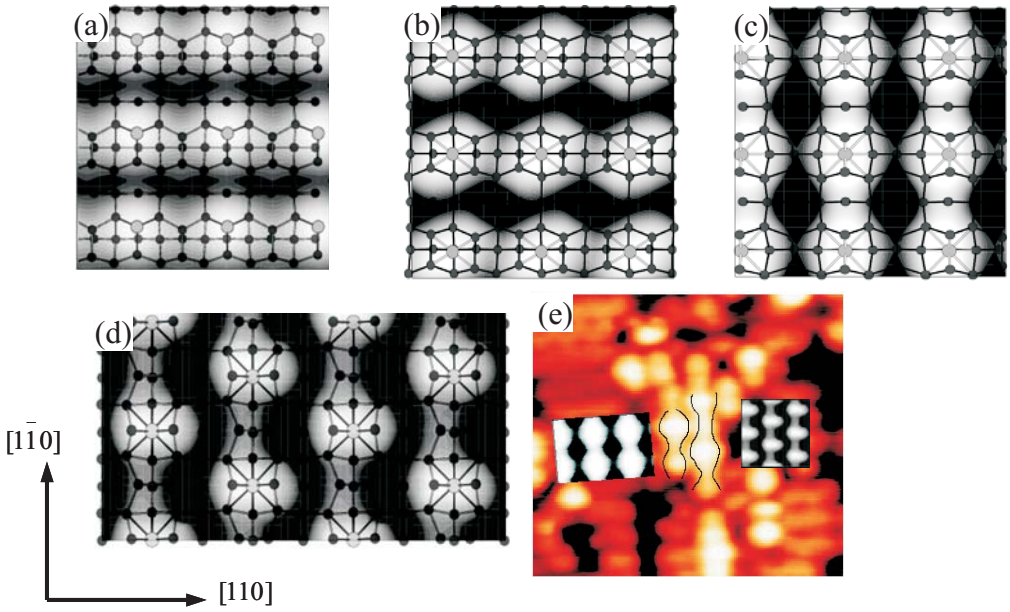

Fig. 5.6: Simulated STM images for single atom adsorption on: substitutional site (a), hollow site (b), interstitial p(2×2) unit cell (c), interstitial c(2×4) unit cell (d), and the experimental STM (e) Ref. [2].

between Mn-Si which appears as a bright protrusion in the STM image. The dark area is the region between dimer rows and the rest funnel-shape parts are π-states in the Si-Si dimers.

The simulated STM images for Mn in substitutional and hollow sites, Fig. 5.6-a and b, show bright and dark stripes in the [110] direction which are parallel to the surface dimer rows. The bright regions are always around Mn atoms and their shape depends on the bonds between Mn and the surface Si atoms. The substitutional site around Mn is protruded while the other dimer is recessed which is the effect of the charge distribution around Mn.

However, in the interstitial site, Fig. 5.6-c, the elongated dimer is shifted up, which causes the distribution of occupied states to be concentrated between dimers rows in the [1$\bar{1}$0] direction. Therefore the STM images show the upper dimer as a bright part while the position of other dimer appears dark, Fig. 5.6-c,d. In this structure there is no strong bond between the other Si-dimers and Mn.

In the c(4×2) interstitial model, Fig. 5.6-d, the strips are still in the [1$\bar{1}$0] direction but the protruding parts are shifted relative to each other which is similar to the experimental STM image, (see Fig. 5.6-e). The experimental image is obtained for a 2.4 V tip bias voltage and 0.03 ML coverage of Mn.

The STM pattern for Mn in the interstitial site looks symmetric in the direction parallel to dimer bonds in both (2) and $c(4 \times 2)$ surface reconstructions.

More details of the bright part related to islands in experimental STM image and theoretical STM simulations are shown in Fig 5.7. A surface, where Mn sits in a c(4x2) structure below the Si-dimers, is clearly different from the STM picture of a clean, c(4x2) reconstructed Si surface, (see Fig. 4.10-a,c in Chap.4).

Figure 5.7-c and d, shows the experimental [2] and simulated curves of the height difference between the islands and the bare surface. A linescan is plotted which crosses the island in the STM images (see Fig. 5.7-a,b). In the experimental image, the island is built up on the bare surface and has a height of about 1.1-1.2 Å.

The three central peaks which are marked by A, B and C, are reproduced by the simulation. The central peak is the superposition of two peaks, which come from the two Si atoms which are located above Mn. This is the position of the Si-dimer which is lengthened and is higher than the surranding surface area.

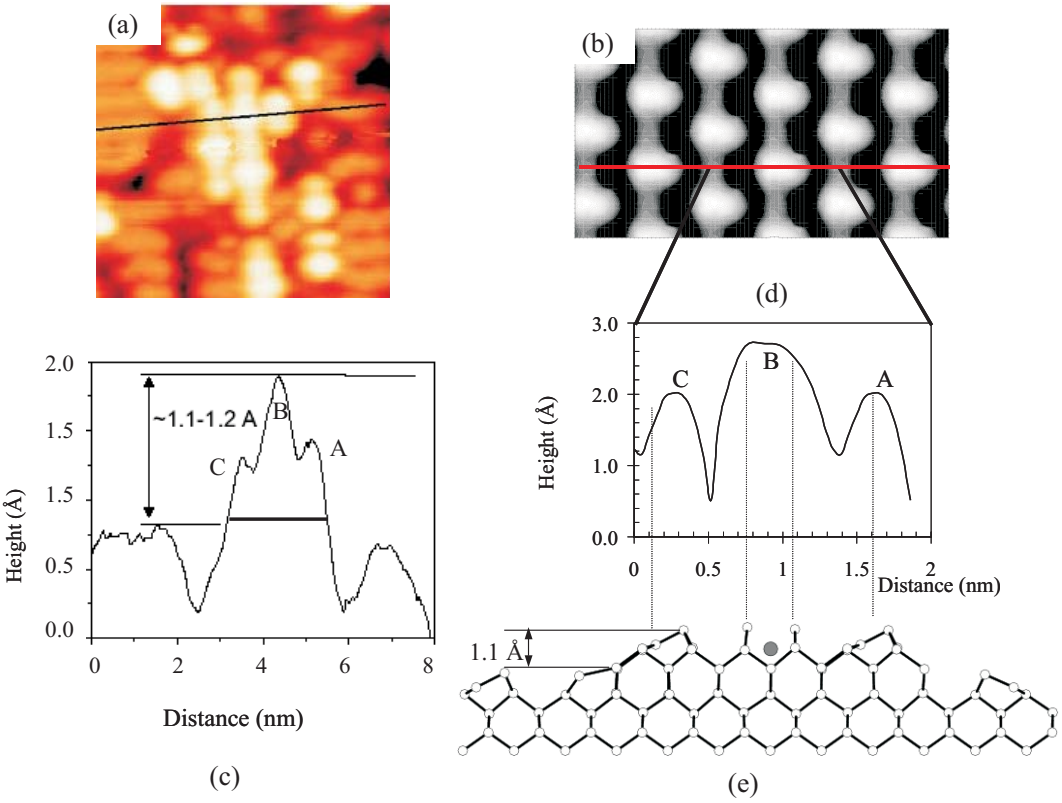

Fig. 5.7: Experimental STM image (a) and theoretical STM simulation (b) for $c(4 \times 2)$ unit cell. Curves (c) and (d) show the height difference in a linescan which runs across the bright part of the STM images. The linescans are indicated in the STM images. (e) ball-stick model of the c(4×2) structure.

The two smaller peaks on the right of and left are intact Si-dimers, which belong to the Si island, and do not contain any Mn (cf. Fig. 5.7-d). The difference in height

between the large and the small peak amounts to about 0.6 Å which is in good agreement with the measurement.

The two regions on the right of and left of the central peaks in the linescan which appear approximately 1.1 Å lower than the maximum, belong to the substrate (cf. Fig. 5.7-c).

5.4 Influence of The Si-Dimer Vacancy

In the following part, the role of surface imperfections on Mn adsorption is investigated. The most abundant defect on a Si(001) surface is the missing-dimer defect [140]. It would be interesting to check the formation of a Mn-decorated missing-dimer defect.

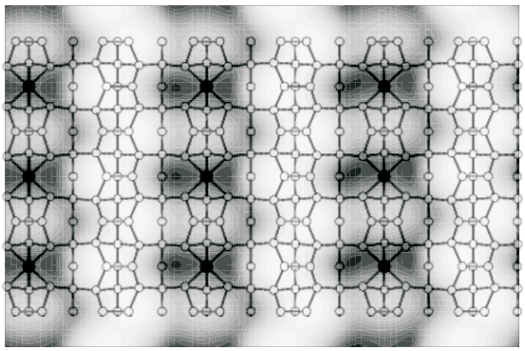

Fig. 5.8: STM simulation of Mn impurity at the position of a dimer vacancy in a (4×2) unit cell matched with a ball-and-stick model.

For Mn atoms occupying the dimer vacancy, first a Si-dimer must be removed, then Mn replaces it. In order to describe the surface with a missing-dimer defect, a larger unit cell is used, either (2×4) or (4×2). As it was discused before in Chap. 4, the first model is considered as a Si dimer row, consisting of blocks of three Si dimers, interrupted by a dimer vacancy. In the second case of the (4×2) unit cell, the surface consists of continuous rows of Si dimers, alternating with rows where a Si dimer and a dimer vacancy follow each other. The second type of dimer vacancies (single dimers alternating with vacant sites in a row) is more stable by 0.48 eV / unit cell. Therefore, this calculation has been performed in a (4×2) unit cell with 25% dimer defects that means 1/16 ML Mn coverage. The adsorption energy of Mn at the dimer vacancy is calculated to be 4.29 eV for the (4×2) unit cell.

Formation of the defect site with Mn adsorbed becomes exothermic, if it is assumed that the two expelled Si atoms move to kink sites at steps (i.e., to a reservoir at the chemical potential of bulk Si).

In table 5.1, the thermodynamic stability of Mn adsorption on the Si-dimer vacancy structure are compared to the adsorption of Mn atom on the perfect Si surface. The

Mn adatom binds very strongly to vacancy site, with a binding energy of 1.4 eV larger than the binding energy at the hollow site. The Mn-atom binds clearly more strongly to the missing-dimer defect than to the normal Si surface. When it (the Mn atom) occupies the dimer vacancy, it comes very close to the surface and sits at about the same height as the Si dimers.

This case is similar to adsorption of Co on Si(001) [132]. Due to Mn-Si bonds the nearset Si-dimers become shorter and more horizontal. The Mn is rather highly coordinated with formation of 6 short Mn-Si bond. In this site Mn placed in the 2nd layer has a magnetic moment of 2.9 μ_{B} which shows strong bonding between Mn and Si.

The STM image is simulated for the energy of -0.5 eV below the Fermi level (filled state), and an iso-surface is plotted with constant charge density of 10^{-6} / Å^3. The perfect dimer rows have a zig-zag shape protrusion pattern similar to the bare Si-surface. In the imperfect dimer rows, the white parts come from the Si-dimer while the dark parts belong to the Mn atom. The Si-dimer in the imperfect row is almost horizontal and about 0.7 Å higher than the Mn impurity.

5.5 Potential Energy Surface for Mn on Si(001)

In the previous section, the stable and meta-stable adsorption sites of Mn on Si(001) were discused. For a detailed study of adatom kinetics, the adatom diffusion pathways and energy barriers should be determined.

Diffusion of adatoms is one of the microscopic processes which controls epitaxial growth on the surfaces. The adsorbed atom binds on the surface at specific sites, exactly at the position of lowest potential energy for the adsorption. This adatom may be able to move from a binding site to an equivalent one without very much expenditure of energy. Therefore the adatom motion is stochastic in a two-dimensional random walk. The mean square displacement is proportional to the time and to the diffusion coefficient , D ($\langle r^2 \rangle \propto Dt$) [141, 142].

The rate of a microscopic process that may take place during diffusion which is proportional to the diffusion coefficient, can be calculated from:

$$\Gamma = \Gamma_0 \exp\left(\frac{-E_d}{k_B T}\right) \tag{5.2}$$

where Γ_0 is the pre exponential factor. The diffusion constant depends on temperature, jump length, and the adatom and substrate vibrations [141, 143]. T and k_B are temperature and Boltzmann constant, respectively. E_d is the energy barrier which

is the energy difference between the maximum (saddle point) and the minimum (equilibrium site) of the potential curve along the diffusion pathway.

In the description of surface adatom diffusion within the transition-state theory (TST) [144] framework it is important to have information about the potential energy surface (PES).

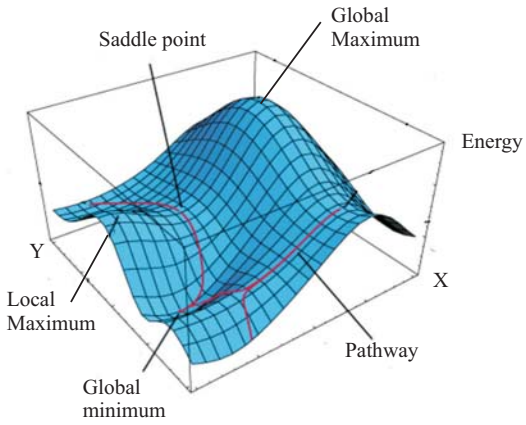

Fig. 5.9: Schematic of potential energy surface. x and y are coordinates of adatom and z axis is adsorption energy.

In order to have a complete map of all binding sites and diffusion pathways one needs to calculate the ground state total energy of the adsorbate system for a dense mesh of adatom positions. This is the so-called potential energy surface.

The energy surface is mapped out in the following way. The adatom is placed at a number of positions (x, y) on the surface. The dimer row is parallel to the y-axis, and the direction of the dimerization bond is along the x-axis. These positions form an equidistant grid with a spacing between the grid points of about 1 Å in x and y directions. Starting with the adatom above the surface, at each (x, y) position the total energy is minimized simultaneously with respect to the electronic charge density and the remaining ionic degrees of freedom, i.e. the x and y coordinates of the adatom and the positions of the two inner layers are fixed.

The minimum of the energy with respect to the z-coordinate of the adatom and all coordinates of the substrate atoms is as follow:

$$E^{\mathrm{PES}}(X_{ad}, Y_{ad}) = \min_{\mathbf{R}} \min_{Z_{ad}} E^{\mathrm{tot}}(\mathbf{R}, \mathbf{Z}_{\mathrm{ad}}) - \mu_{\mathbf{ad}} \mathbf{E}^{\mathbf{bulk}}_{\mathbf{ad}} \tag{5.3}$$

Here R denotes the position of the substrate atoms, μ is chemical potential and N is the number of each type of atom in the unit cell.

The global (local) minimum in the PES corresponds to the stable (meta-stable) binding positions of the adatom, and saddle points correspond to transition states for adatom diffusion.

In the description of an adatom on a surface within the framework of transition-state theory, it would be necessary to determine the energy barrier for a jump be-

tween two binding sites. One should locate the maximum energy along each possible path in the complete configuration space which connects the configurations of two binding sites. The minimum energy among these maxima is the energy barrier for diffusion and the total-energy function then has a saddle point at the corresponding configuration.

The minimum value of the energy barrier of different pathways between two minima is the so-called diffusion barrier.

We note that important binding sites and transition states could be missed in the so-defined PES, *e.g.*, sub-surface sites that cannot be reached by relaxing the adatom from above the surface. In this case, additional computational work has to be done to obtain the complete picture.

Usually, the pathway with the lowest energy barrier will be used most frequently, but other pathways may exist which have comparable barrier and contribute with less probability [145]. Therefore, the effective barrier should be measured by averaging over all possible pathways with respect to their probability.

Lastly,the combination of DFT calculations and kinetic Monte Carlo simulations describe and analyze epitaxial growth.

In order to have complete information about surface diffusion and sub-surface penetration barriers, two PES are mapped and several diffusion pathways are considered in the following part.

5.5.1 PES and Diffusion Pathway on The Surface

The potential energy surface for a Mn adatom *on* the Si(001) surface is mapped in Fig. 5.10. The energy minima were found by explicit energy minimization with respect to x and y. The saddle points were pinpointed by interpolating the PES on a finer grid of points.

The binding position of the adatom, H, is the absolute minimum on the surface. There is a local minimum on the x axis which is 0.3 eV higher than the energy of the absolute minimum. There is a pathway connecting the absolute minima of two adjacent cells by passing through this point.

As was discussed before, the Mn atom binds most strongly at the hollow site (marked by H in Fig. 5.1), also called pedestal site by other authors, [124] located between two Si surface dimers. At this site, the Mn adatom makes bonds with all four neighboring surface Si atoms, while the Si–Si dimer bonds are elongated. The adatom in the global minimum (H) is 0.2 Å above the surface and the tilt angle slop of the buckled Si-dimers is reduced significantly.

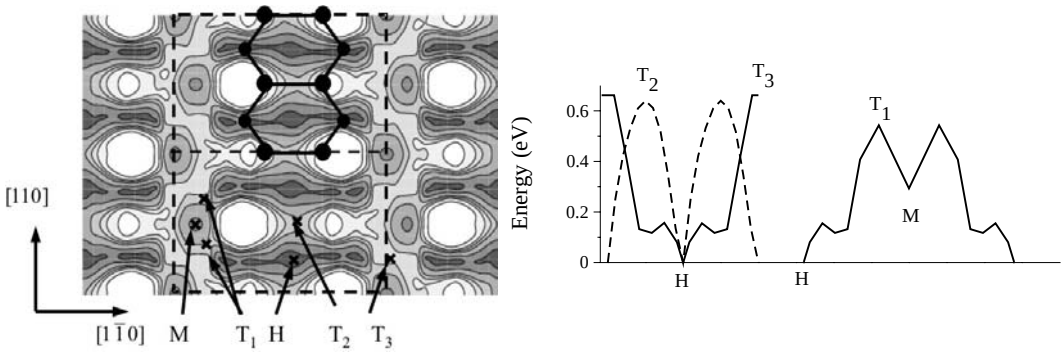

Fig. 5.10: The PES and diffusion pathway on the Si(001) surface. The diffusion barriers for hopping to the next on-surface minimum are in the range of 0.6 eV. H and M are global and local minimum, T_1, T_2 and T_3 are saddle points. The white region are maximum and the dark parts are minimum in the potential energy surface. The space between contour lines is 0.2 eV.

In the weaker binding site (M in Fig. 5.10), the Mn adatoms interacts with the (occupied) dangling bond of the upper Si atom in the surface Si dimer.

There are three diffusion routes for Mn on the surface:
1) An indirect pathway via the minimum M, passing twice through symmetry-equivalent saddle points T_1 with energy barrier of 0.55 eV.
2) A pathway which runs parallel to the dimer rows which crosses the dimer short bridge site (T_2).
3) A pathway perpendicular to the dimer rows that runs between two adjacent dimers in the neighboring rows (T_3).

The first outcome is that the diffusion barriers along pathway (T_2) and (T_3) are almost the same with 0.65 eV which indicates isotropic diffusion in parallel and perpendicular to the dimer rows. On the contrary, for diffusion of a Si atom this surface behaves anisotropic with 0.6 eV and 1.0 eV energy barrier along and perpendicular to the surface dimer rows, respectively [146].

5.5.2 PES and Diffusion Barrier for Penetration to The Sub-Surface (site I_1)

It is well known that Mn in bulk silicon is a mobile impurity which occupies preferentially interstitial sites. [147, 148] For this reason, it could be expected that sub-surface sites, in addition to on-surface sites, play a role for Mn adsorption and diffusion, and we consider this possibility in this Section.

The second-layer interstitial site below the Si dimer, I_1, is the most stable site for Mn, Fig. 5.1. With 3.8 eV adsorption energy it is actually lower in energy than any

surface site. Now the question arises how Mn diffuses on this surface to reach the sub-surface site and how high the energy barrier for penetration to the sub-surface is.

Determining the diffusion pathway requires special care, because considerable relaxation of the neighboring Si atoms occurs along the pathway. For this reason, we plotted the PES for a Mn atom in a $[1\bar{1}0]$ plane perpendicular to the surface, which intersects both the hollow and the interstitial sites. We fix the Mn atom at a set of positions in this plane, and relax the substrate Si atoms in each case. The resulting PES, spanned by [110] and [001] vectors, is displayed in Fig. 5.11. It is seen that for the most favorable pathway the Mn adatom first moves slightly upward away from the hollow site. Thereby, the surface Si dimer is elongated, thus giving room for the Mn atom to find its way to the sub-surface interstitial site. The energy barrier for the penetration pathway H-T-I_1, crossing the transition state T, is about 0.3 eV measured from the hollow site, and about 1.2 eV for the reverse process (see Fig. 5.11-b).

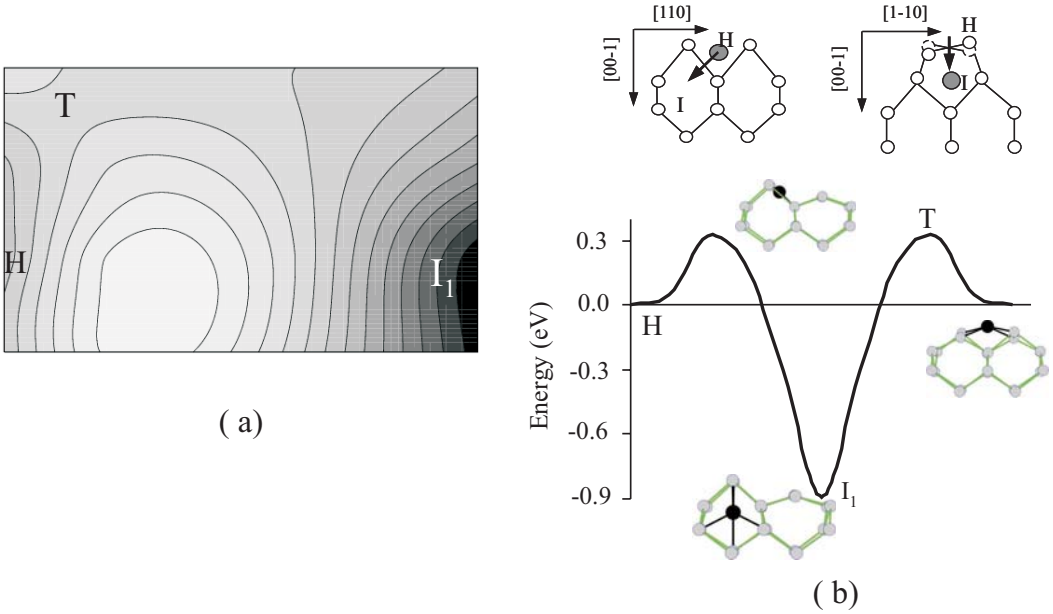

Fig. 5.11: PES plot and diffusion barrier for penetration to the sub-surface site (a). The energy barrier is about 0.3 eV. The dark region is the global minimum and the bright part is the place of maximum in the PES. Structure of minimum and saddle points are shown in figure (b). The space between contour lines is 0.125 eV.

In addition, one can consider the possibility that a Mn atom coming from the vacuum could directly reach the second-layer interstitial site, by normal incidence and breaking of the Si dimer. For these calculations, a $c(4 \times 2)$ unit cell is used , in order to avoid spurious interactions between neighboring Si dimers being broken, which could occur if a $p(2 \times 2)$ cell would be used for simulating this process. The calcula-

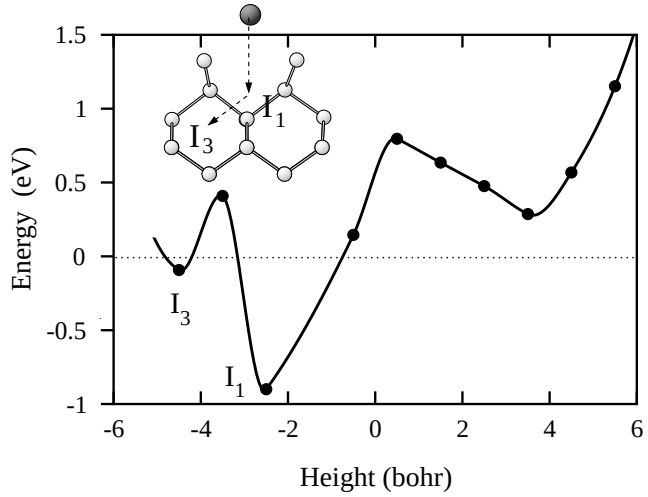

Fig. 5.12: Energy profile for a Mn atom approaching the Si(001) surface from the vacuum along the path shown in the left panel, breaking the Si dimer and inserting itself via the stable sub-surface site I_1 into the third-layer interstitial site I_3. The energy barrier for the last step, from I_1 to I_3, is about 1.3 eV.

tions show that the energy of this system first decreases when Mn approaches the surface, but then rises again by about 0.5 eV and goes through a maximum before decreasing finally to the binding energy in the interstitial site (Fig. 5.12).

The intermediate increase in energy is associated with the Mn atom breaking the Si-Si dimer bond. However, the energy gained by the Mn atom during approaching the surface is more than sufficient to overcome this energy barrier. Hence we conclude that a deposited Mn atom can reach the interstitial site both indirectly through the hollow site, or directly by breaking the Si dimer upon impact, if the site and angle of impact are appropriate, but the indirect approach is faster because of the lower barrier. The possibility of such a direct process was also demonstrated by calculations for Mn on GaAs(001). [138]

The results of Dalpian *et al.* are in good agreement with the present work, except for the energy barrier between the hollow site and the sub-surface interstitial site, which we find to be 0.3 eV while they reported a higher value of 0.96 eV .

The behavior of Mn on Ge (001) is similar to Si (001) [123]. The adatom penetrates to the 2nd layer interstitial site via the hollow site. Zhu *et al.* reported an energy barrier of 0.59 eV and the reverse process barrier is 1.22 eV, which is comparable with results for Si in this work. Also for Ge, the deeper layer interstitial and substitution sites are less stable than the 2nd layer interstitial site.

In deposition of Mn on GaAs(001) the interstitial site below the As dimer is also the most stable site for Mn on GaAs(001) [138]. Mn with 0.2 eV energy cost breaks the

dimer and penetrates to the sub-surface. In GaAs the cave site is a stable site and the energy barrier to reach this position is almost zero. This site is located between two adjacent dimers above a Si atom in the fourth layer. In contrast to GaAs, the cave site is an unstable adsorption site for Mn on Si(001). The Mn atom moves up from this position to the surface site, M, which is a local minimum in the PES (see, fig. 5.1 and 5.10), without any barrier.

The present calculations show that there are high energy barriers for diffusion of Mn into deeper layers. To reach the third-layer site, Mn must overcome an energy barrier of 1.3 eV, measured from the second-layer interstitial site (Fig. 5.12).

Moreover, it is concluded that Mn atoms, even after penetrating to the sub-surface site, will diffuse mainly through the on-surface (H) site to find other Mn atoms for nucleation of some silicide, rather than through a bulk diffusion mechanism.

The diffusion barriers of Mn in Si bulk reported in the literature are around 1.3 eV [147] and 1.17 eV (theory) [137].

5.6 Effect of Adatom Interaction : Submonolayer, Overlayer, or Bilayer Structures

In a hierarchy of growth, the adsorption of Mn at higher coverage, in the range between 1/4 and 1 ML will be studied. With the choice of the (2×2) cell, this corresponds to adsorption of 2–8 Mn atoms per supercell.

For two Mn atoms, one possibility is the adsorption at adjacent interstitial and hollow sites. This geometry is found to be the most stable arrangement for a pair of Mn atoms in the present calculations. Other configurations that can be realized by two Mn atoms in the $p(2 \times 2)$ cell correspond to infinite chains of Mn adatoms. Chains in the [110] direction (along the dimers rows) can be formed in two ways, either by occupation of all on-surface hollow sites, or by occupation of all sub-surface interstitial sites.

It is found that the adsorption energy per Mn atom in an infinite chain is larger than for a single atom per unit cell for the hollow site, while for the interstitial site the infinite chain has a lower absorption energy compared to single Mn atoms. In other words, Mn adatoms in hollow sites interact attractively, whereas Mn atoms in the interstitial site show a repulsive interaction. This can be understood from the fact that Mn atoms in interstitial sites introduce tensile strain by widening the Si crystal lattice in their neighborhood, and hence two interstitial Mn atoms repel each other through these strain fields. However, a chain of interstitial Mn atoms is still lower in energy than the chain of hollow site Mn atoms; i.e., the trend for

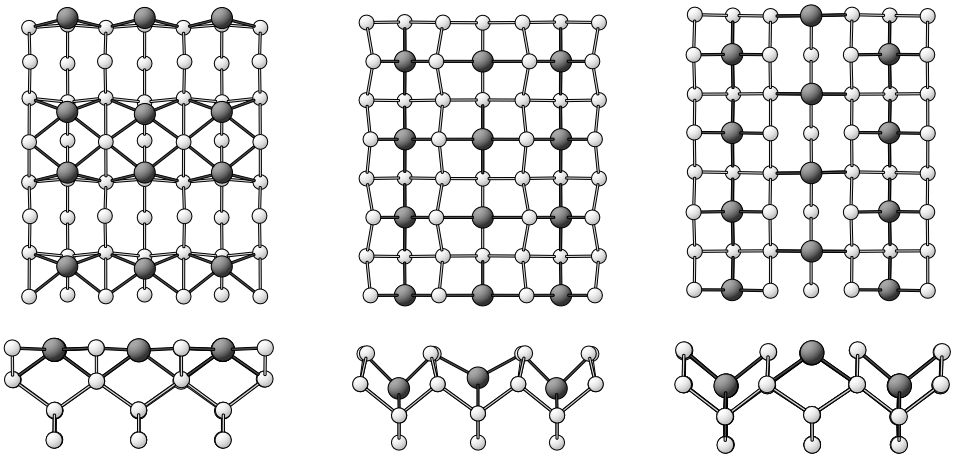

Fig. 5.13: Different possible structures for adsorption of 1/2 ML of Mn on Si(001), shown in top view (upper panels) and side view (lower panels). (a) relaxed structure resulting from Mn in on-surface sites only (b) in sub-surface sites (c) in sub-surface and cave sites.

occupying sub-surface positions persists.

Furthermore, chains of on-surface Mn atoms in $[1\bar{1}0]$ direction perpendicular to the Si dimer rows are considered. Alternately one Mn atom is in a hollow site, and one Mn atom is in a cave site. Although the adsorption energy per atom is less than the average adsorption energy of these two sites calculated separately (i.e., there is attractive interaction), this chain is energetically less favorable than any chain of Mn atoms running in [110] direction.

For coverage 3/8 ML, i.e., 3 Mn atoms per unit cell two possibilities are studied:
For on-surface adsorption a chain of Mn atoms in hollow sites, plus one Mn atom in a cave site is considered.
For sub-surface adsorption a chain of interstitial Mn atoms, plus one Mn atom occupying a hollow site on the surface is supposed to form.
As for the 1/4 ML case, the latter possibility, combining interstitial and hollow sites, is energetically more favorable. In both geometries, the Si dimers are still intact, albeit elongated.

For a coverage of 1/2 ML there are 4 Mn adatoms occupying both hollow sites and both cave sites of the unit cell. Starting from this geometry, the surface spontaneously transforms to a configuration where each of the Mn atoms has four in-plane bonds to neighboring Si atoms, formerly being part of Si dimers, which have been broken up due to bonding to the Mn atoms. In addition, each Mn atom establishes two bonds to second-layer Si atoms. This structure has a (1×1) periodicity, the same

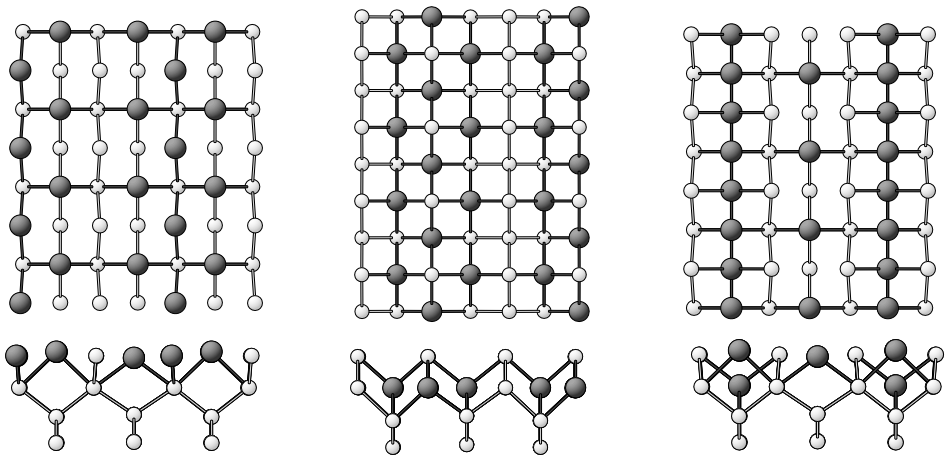

Fig. 5.14: Structures for adsorption of 3/4 ML of Mn on Si(001), shown in top view (upper panels) and side view (lower panels). (a) relaxed structure resulting topmost layer (b) sub-layer with Si-capping layer (c) from 1/2 ML in on-surface sites plus 1/4 ML in sub-surface sites.

as the underlying substrate. The energy of this structure can be lowered slightly if two neighboring Mn atoms move toward each other along the [110] direction, see Fig. 5.13-a. Due to this relaxation, the symmetry of the surface reconstruction is lowered from (1×1) to (1×2), with the long side of the unit cell now along the direction of the former Si dimer row. Alternatively, the case of sub-surface adsorption are also studied. This atomic configuration is obtained by relaxing a structure where Mn atoms are sitting in interstitial sites, and also at cave sites in the trenches between Si dimer rows, the latter Mn atoms either bonding to two third-layer Si atoms (see Fig. 5.13-b), or sitting directly above a third-layer Si atom (cf. Fig. 5.13-c). As a result of the calculations, it is found that at 1/2 ML coverage, on-surface Fig. 5.13-a and sub-surface Fig. 5.13-b adsorption yield the same energies within numerical accuracy, while the mixed structure shown in Fig. 5.13-c gives an energy lower by about 0.24 eV per adatom.

Upon further increasing the number of Mn atoms in the mixed Mn-Si layer, the system has the tendency to adsorb the additional Mn atoms by a mixed occupation of both sub-surface and on-surface site (cf. Fig. 5.14-c) rather than in the sub-surface layer, Fig. 5.14-b, and topmost layer, Fig. 5.14-a . This configuration, is also found to be energetically more favorable by about 0.06 eV per atom than an alternative when Mn substitutes for the atoms in the sub-surface layer.

For the magnetic coupling of Mn atoms in the same layer, the antiferromagnetic ordering is found to be energetically preferred by about 0.05 eV per atom compared

to ferromagnetic ordering. For mixed structures with $\theta = 3/4$ ML, the energy difference between two possibilities where the dense Mn layer is the topmost layer or in the sub-surface is calculated. The first configuration is lower in energy by 0.11 eV.

Table 5.2: Average adsorption energies per Mn atom of ordered monolayer structures at various Mn coverages θ with respect to bulk Mn and bulk Si. The left column is for all Mn atoms occupying on-surface (H) sites, and the middle column is for all Mn atoms in sub-surface (I_1) sites, the right column is for structures where sub-surface (I_1) and on-surface (H) sites are alternatingly populated.

Mn coverage (ML)	on surface eV / Mn	sub-surface eV / Mn	sub+on surface eV / Mn
$\theta = 1/8$	2.91	3.8	—
$\theta = 2/8$	3.01	3.4	3.44
$\theta = 3/8$	3.32	3.31	3.40
$\theta = 4/8$	3.29	3.31	3.55
$\theta = 6/8$	3.06	3.45	3.52

The results for adsorption of 1/8 ML up to 6/8 ML of Mn are summarized in Tab. 5.2, quoting the average adsorption energy per Mn atom. The mixed occupation of sub-surface and on-surface sites is found to be most favorable, and leads to a monotonous decrease of the energy per atom during the increase of coverage. In contrast, occupation of on-surface sites only is energetically less favorable. Hence, the former growth mechanism, alternating occupation of sub-surface and on-surface sites, is identified as the preferred mechanism for growth of MnSi islands on Si(001).